

Generating scalable entanglement of ultracold bosons in superlattices through resonant shakingLushuai Cao,^{1,*} Xing Deng,¹ Qian-Ru Zhu,¹ Xiao-Fan Xu,² Xue-Ting Fang,¹
Xiang Gao,¹ Peter Schmelcher,^{3,4} and Zhong-Kun Hu^{1,†}¹*MOE Key Laboratory of Fundamental Physical Quantities Measurement, Hubei Key Laboratory of Gravitation and Quantum Physics, School of Physics, Huazhong University of Science and Technology, Wuhan 430074, People's Republic of China*²*Institute of Space-based Information System, China Academy of Electronics and Information Technology, Beijing 100041, People's Republic of China*³*Zentrum für Optische Quantentechnologien, Universität Hamburg, Luruper Chaussee 149, 22761 Hamburg, Germany*⁴*The Hamburg Centre for Ultrafast Imaging, Luruper Chaussee 149, 22761 Hamburg, Germany*

(Received 5 December 2017; published 25 June 2018)

Based on a one-dimensional double-well superlattice with a unit filling of ultracold atoms per site, we propose a scheme to generate scalable entangled states in the superlattice through symmetry-protected resonant lattice shaking. Our scheme utilizes periodic lattice modulations with a specific two-body exchange symmetry to entangle two atoms in each unit cell with respect to their orbital degree of freedom, and the complete atomic system in the superlattice becomes a cluster of bipartite entangled atom pairs. To demonstrate this we perform *ab initio* quantum dynamical simulations using the multilayer multiconfiguration time-dependent Hartree method for mixtures, which accounts for all correlations among the atoms. The proposed clusters of bipartite entanglements manifest as an essential resource for various quantum applications, such as measurement-based quantum computation. The lattice shaking scheme to generate this cluster possesses advantages such as a high scalability, fast processing speed, rich controllability on the target entangled states, and accessibility within current experimental techniques.

DOI: [10.1103/PhysRevA.97.063620](https://doi.org/10.1103/PhysRevA.97.063620)**I. INTRODUCTION**

Ultracold atoms in optical lattices, which benefit from their almost perfect decoupling from the environment and their excellent tunability [1,2], have become a promising platform for realizing quantum entanglement with related applications, such as quantum metrology [3] and quantum computation [4,5]. There have been various protocols for quantum computing with ultracold atoms, among which the measurement-based quantum computation (MBQC) [6] is particularly suitable for lattice atoms. The MBQC is incorporated with two elementary steps, including the preparation of scalable multiparticle entangled states [7,8] and operations of local quantum gates on the entangled states. Various generation schemes have been proposed or even experimentally realized for multiparticle entangled states, such as those based on controlled collisions [4,9,10] and superexchange interactions [11–16], among which the entanglement is mainly encoded into the internal degree of freedom (DOF) of the atoms. There is now also a growing interest to use the orbital DOF [17] of lattice atoms for quantum computations, which possesses advantages such as insensitivity to external magnetic fluctuations and high controllability by lattice modulations. Various quantum gate operations have been proposed for the orbital DOF [18–22] and it demands an efficient scheme to generate scalable multiparticle entangled states with respect to the orbital DOF to accomplish a complete MBQC.

The orbital DOF has a relatively short coherence time, mainly due to the spontaneous decay of higher orbitals, and

schemes involving second-order hoppings become unsuitable for generating entanglement with respect to the orbital DOF. Recently, lattice shaking has become a powerful tool to manipulate ultracold atoms in optical lattices [23–28] and it offers a direct access to the orbital DOF. Site-resolved lattice shaking has already been used to design local quantum gates operating on the orbital DOF [21]. In this work we propose a lattice shaking scheme, which can efficiently generate scalable lattice entanglement encoded into the orbital DOF with a single operation. The generated entangled states can be directly applied for MBQC, which makes the lattice shaking scheme an elementary ingredient for MBQC with quantum information encoded in the orbital DOF.

This paper is organized as follows. In Sec. II we present the setup under consideration, in Sec. III the preparation scheme for target entangled states, and in Sec. IV the numerical method for the simulations. In Sec. V we show the numerical evidence for the preparation scheme in terms of the validity and accuracy (Sec. VA), the flexibility (Sec. VB), and the efficiency (Sec. VC). A brief summary and discussion are given in Sec. VI.

II. SETUP

We consider a one-dimensional (1D) double-well superlattice loaded with contact interacting bosons, with a unit filling per site, i.e., two bosons per unit cell. The corresponding Hamiltonian reads

$$H_0 = \sum_{i=1}^{2N} \left(\frac{-\hbar^2}{2M} \partial_{x_i}^2 + V_{\text{sl}}(x_i) \right) + \sum_{i < j=1}^{2N} g \delta(x_i, x_j), \quad (1)$$

*lushuai_cao@hust.edu.cn

†zkhu@hust.edu.cn

which describes $2N$ atoms of mass M confined in a 1D double-well superlattice of N unit cells. In Eq. (1), i and j label the bosons, with the corresponding coordinates denoted by x_i and x_j , respectively. The superlattice is given by $V_{\text{sl}}(x) = V_0[\sin^2(kx/2) + 2\cos^2(kx)]$, which can be formed by two pairs of counterpropagating laser beams of wave vectors k and $k/2$, respectively. In this work we consider a deep superlattice with $V_0 = 10E_R$, where $E_R \equiv \hbar^2 k^2 / 2M$ is the recoil energy, and each site possesses at least two well-defined single-particle states, named the s and the p orbital, with the energy around $8.8E_R$ and $16.4E_R$, respectively.

III. TARGETED ENTANGLED STATES AND PREPARATION SCHEME

Employing a corresponding interaction strength, the ground state of the system is a Mott-like state, in which to a certain approximation each atom occupies a separate site, residing in the lowest orbital, i.e., the s orbital of the site. This ground state can be described as

$$|G\rangle = \prod_{i=1}^N |s, s\rangle_i, \quad (2)$$

where $|\alpha, \beta\rangle_i$ denotes that two atoms occupy the i th unit cell of the superlattice, one in the α orbital of the left site and the other in the β orbital of the right site of the cell. The targeted entangled states are chosen as

$$|\pm\rangle = \prod_{i=1}^N \frac{1}{\sqrt{2}} (|s, p\rangle_i \pm |p, s\rangle_i). \quad (3)$$

Both $|+\rangle$ and $|-\rangle$ correspond to an entangled state, of which the two atoms in the same unit cell become entangled with respect to their orbital DOF, with only one atom in the cell occupying the p orbital and the other remaining in the s orbital. Residing in states $|\pm\rangle$, the complete system becomes a cluster of bipartite entangled pairs in each unit cell. To a good approximation, $|\pm\rangle$ are degenerate eigenstates of H_0 and this ensures that the system can stay stable in the entangled state after the generation scheme, which will be of benefit to further operations on the entangled states, such as the quantum gate operations.

It is natural to think of using resonant shaking to excite $|+\rangle$ or $|-\rangle$ from $|G\rangle$, in which case the shaking frequency matches the energy difference between $|G\rangle$ and $|\pm\rangle$. However, an intrinsic difficulty of this approach is the degeneracy of $|+\rangle$ and $|-\rangle$, which prevents a controllable selective excitation of $|+\rangle$, $|-\rangle$, or their on-demand superposition by an arbitrary shaking potential. To circumvent the degeneracy-induced difficulty, we exploit a particular two-body exchange symmetry of $|G\rangle$ and $|\pm\rangle$ and propose a symmetry-protected resonant shaking scheme (SPRSS) for the selective excitation of $|\pm\rangle$ from $|G\rangle$. This symmetry is related to the two-body exchange operator $\hat{T} : x_1 \leftrightarrow -x_2$ acting on the two bosons confined in the same unit cell, where $x_{1(2)}$ denotes the atomic coordinate with the origin taken at the center of the cell. It can be proven (see Appendix A) that $\hat{T}|G\rangle = |G\rangle$ as well as $\hat{T}|\pm\rangle = \mp|\pm\rangle$, and shaking potentials fulfilling $\hat{T}V_s\hat{T}^\dagger = +V_s$ ($\hat{T}V_s\hat{T}^\dagger = -V_s$) can exclusively couple $|G\rangle$ to $|-\rangle$ ($|+\rangle$). Guided by this symmetry consideration, we have identified two potentials

capable of performing a selective excitation of $|\pm\rangle$:

$$\begin{aligned} V^+(x, t) &= V_+ \sin(\omega t) \sin(kx/2), \\ V^-(x, t) &= V_- \sin(\omega t) \cos^2(kx). \end{aligned} \quad (4)$$

Provided that $\hat{T}V^{-(+)}\hat{T}^\dagger = +(-)V^{-(+)}$, the resonant shaking $V^{-(+)}$ can selectively excite the system from $|G\rangle$ to $|-\rangle$ ($|+\rangle$). Moreover, a combination of V^+ and V^- can generate an on-demand superposition of $|+\rangle$ and $|-\rangle$, which resembles a rotation quantum gate and adds to the flexibility of the SPRSS. The 1D double-well superlattice and the shaking potentials V^\pm are illustrated in Fig. 1.

IV. NUMERICAL METHOD

To demonstrate the validity and efficiency of SPRSS, we perform *ab initio* fully correlated numerical simulations of the dynamical process of shaking. The method applied here is the multilayer multiconfiguration time-dependent Hartree method for mixtures (ML-MCTDHX) [29–31], which has been developed from multiconfiguration time-dependent Hartree and related methods [32–37] and works equivalently to the multiconfiguration time-dependent Hartree method for bosons (MCTDHB) [36–38], when handling a single-species system of indistinguishable bosons. The ML-MCTDHX accounts for all correlations among the bosons and can intrinsically take into account the exact geometry of the 1D superlattice and the parity of the shaking potentials, which turns out to be essential for the generation scheme in this work. The atoms in the superlattice are taken as a closed system, and effects due to finite but sufficiently low temperature and/or spontaneous emission are ignored, which, however, we believe will not affect the main results of this work.

Besides a complete characterization of quantum correlations of the system, the ML-MCTDHX also takes advantage of the temporal optimization of the Hilbert space truncation to achieve reliable simulation results. Particularly during shaking, some highly excited states can be populated through multiphoton absorption processes and intermediate higher-order dynamics. Such highly excited states could be easily ignored by static truncations and it is hard to determine *a priori* the Hilbert space truncation with respect to these highly excited states. The ML-MCTDHX and related methods can avoid, to a great extent, this danger by the temporal optimization of the Hilbert space truncation, which could automatically activate the population of necessary quantum states involved in the dynamics, as long as the convergence is ensured. This unique advantage makes the ML-MCTDHX and related methods most suitable for simulations of quantum dynamics, particularly under shaking. For more details on the ML-MCTDHX and its convergence, we refer the reader to Appendixes B and C.

V. NUMERICAL RESULTS

A. Validity and accuracy

We now present evidence for the validity, accuracy, flexibility, and efficiency of the SPRSS with V^\pm by performing *ab initio* simulations via the ML-MCTDHX. Concerning the validity and accuracy, we mainly focus on two aspects of the scheme: (i) Within a unit cell the lattice shaking is able to

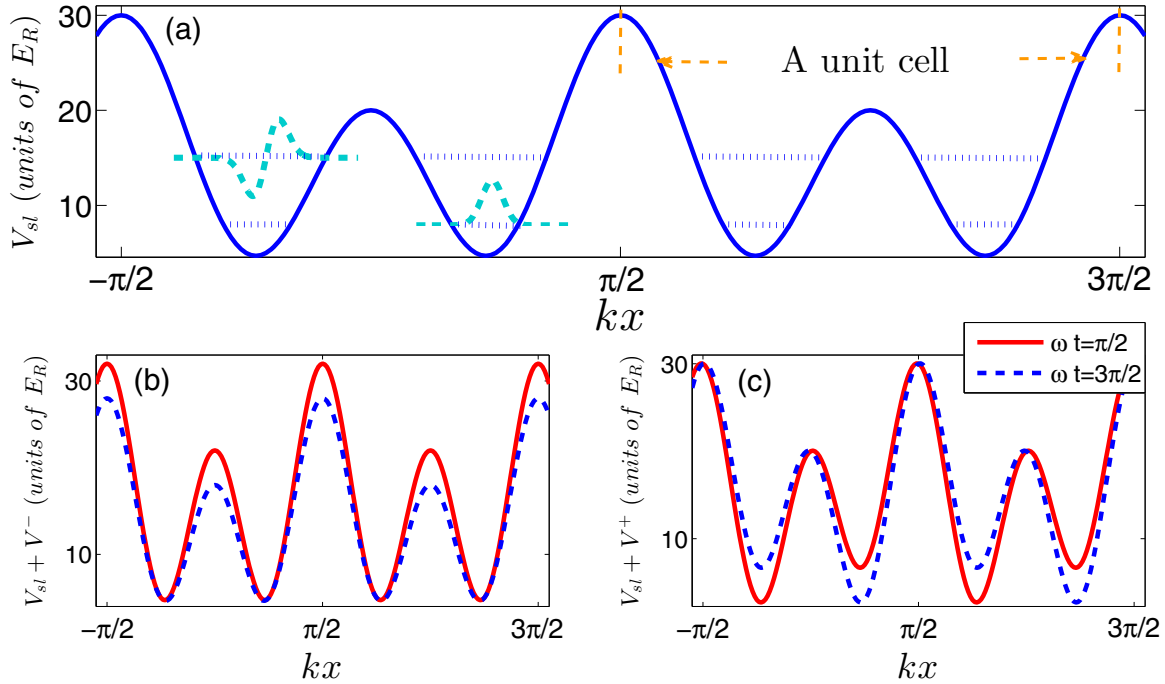


FIG. 1. Sketch of (a) the double-well superlattice, (b) the shaking potential of V^- , and (c) the shaking potential of V^+ . In (a), the energy levels and the profiles of the s and p orbitals are sketched by the blue dotted and cyan dashed lines, respectively. The potentials V^- and V^+ with the largest shaking amplitudes are shown in (b) and (c), respectively, where it can be seen that V^- provides a shaking of the intersite barriers, whereas V^+ provides a temporal modulation of the energy offset between the left and right sites in a cell.

transfer the initial state to the targeted entangled state and (ii) intercell interactions of neighboring cells will not affect the intracell entanglement. For this purpose, simulations are performed on a homogeneous double-well superlattices with $N = 1, 2, 3$ unit cells, where the intra- and intercell aspects concerning the validity of our scheme can be simultaneously addressed. Periodic boundary conditions are used, which however do not affect the main results discussed here. To characterize the outcome of the shaking process, two quantities are analyzed: the fidelity of the targeted eigenstates $f_{\pm}(t) = |\langle \pm | \Psi(t) \rangle|^2$ [39], with $|\Psi(t)\rangle$ denoting the total wave function of the system, and the two-body correlation function $g^{(2)}(x_1, x_2) = \rho_2(x_1, x_2) / \rho_1(x_1)\rho_1(x_2) - 1$, with $\rho_2(x_1, x_2)$ and

$\rho_1(x_i)$ ($i = 1, 2$) denoting the two-body and one-body densities, respectively. The fidelity provides access to the time evolution of the entangled states during the shaking process, and the procedure to obtain the fidelity in our analysis is introduced in Appendix B. The two-body correlation is used to analyze the generated entangled states, with a focus on the intercell interaction effects.

Figure 2(a) and 2(b) present the results for the potentials V^+ and V^- with $N = 2$ unit cells, respectively. The shaking is applied to the lattice for a finite time period and is immediately turned off when the fidelity of the targeted entangled states reaches a maximum. The profiles of the shaking amplitudes for V^+ and V^- are shown in the upper panels of Figs. 2(a) and

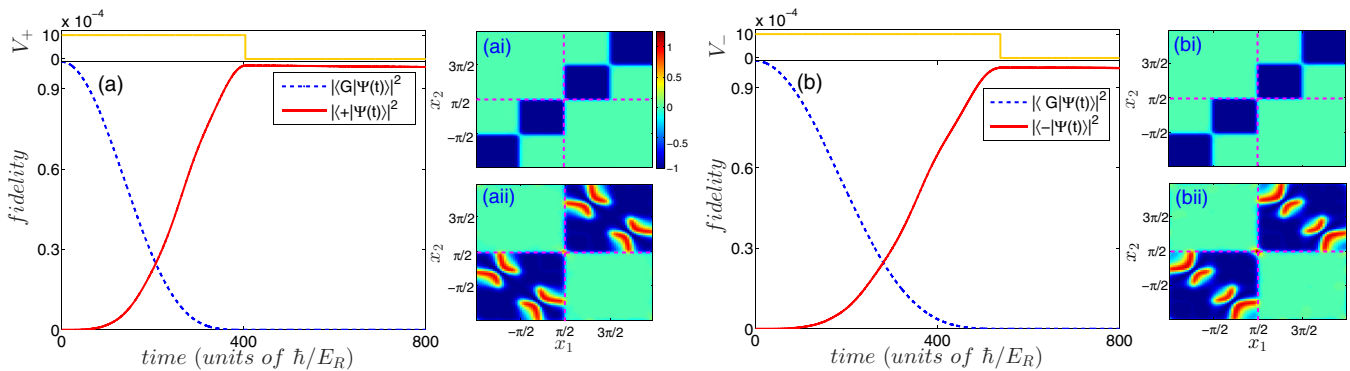


FIG. 2. Fidelity of corresponding entangled state as a function of time, under shaking via (a) V^+ and (b) V^- , with (a) showing the profile of the shaking amplitude, with $V_{+(-)} = 0.001 E_R$ and $\omega = 7.54 E_R / \hbar$. Also shown is the correlation function $g^{(2)}$ at (ai) and (bi) the initial time $t = 0 \hbar / E_R$, (aii) $t = 424 \hbar / E_R$, and (bii) $t = 548 \hbar / E_R$, when the shaking has been turned off. The four insets share the same color bar. The interaction strength is set to $g = 2.5$ here and in the following figures.

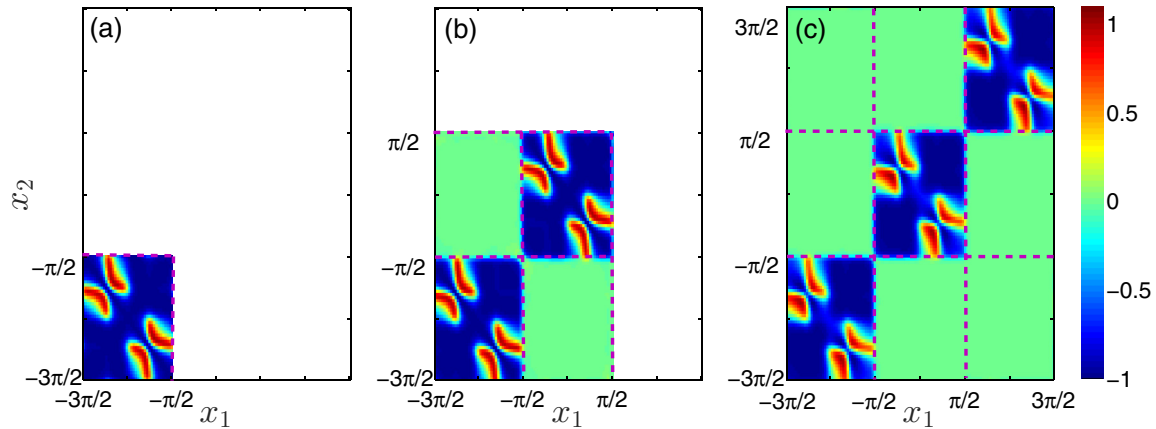


FIG. 3. Two-body correlation function $g^{(2)}$ of the entangled states generated by shaking V^+ for (a) a single-cell, (b) a double-cell, and (c) a triple-cell setup. The spatial interval is set to the range covering a triple-cell lattice for the convenience of comparison and the empty space in (a) and (b) is simply because the corresponding setup does not cover the related spatial interval.

2(b), respectively. In Fig. 2(a), during the shaking with V^+ , the fidelity of $|+\rangle$ monotonically increases, reaching a maximum value. Afterward, the shaking is turned off and the system remains stable in $|+\rangle$. The maximum fidelity of the double-cell system is around 98.6%, indicating that the system resides very well in a product state of bipartite entangled states of the bosonic pairs. The fidelity for the bipartite entanglement in each supercell is then the square root of that of the double-cell system, that is, 99.3%. The $g^{(2)}$ function provides a further indicator of the generation of the entangled states. At the initial time $t = 0 \hbar/E_R$ [Fig. 2(ai)], the system resides in $|G\rangle$ and there is no nontrivial correlation but the antibunching of the atoms in the diagonal blocks indicating the Mott-insulator-like initial state due to the repulsive contact interaction. At a later time when the shaking has been turned off, the two atoms in the same unit cell are entangled, documented by the wings appearing in the intracell correlation blocks. Meanwhile, the intercell correlation remains practically zero for the complete dynamical process, indicating that the intercell influence is vanishingly small on the intracell entanglement generation. Similarly, Fig. 2(b) shows the fidelity and the two-body correlations as a function of time under the lattice shaking of V^- . A maximum fidelity around 98.7% of the bipartite entanglement in each unit cell is reached. For the two-body correlations, the expected wings in the intracell correlation blocks and the vanishing intercell correlations are present. In total, the fidelities and two-body correlations confirm the validity and accuracy of the selective entanglement generation scheme with a lattice shaking of V^\pm .

To further confirm the validity of the SPRSS in a multicell system, we extend the simulations to six bosons in three unit cells to further confirm the vanishing of the intercell correlations. The $g^{(2)}$ functions for the setup of $2N$ bosons in N unit cells with $N = 1, 2, 3$ are shown in Fig. 3. In Figs. 3(a)–3(c) we observe that in the blocks corresponding to the intracell correlations, almost identical biwing profiles are present, which indicates the onset of entanglement within each unit cell. Moreover, the correlations in the intercell blocks are plain and approaching zero, which further confirms the vanishingly small intercell coupling between nearest-neighbor and next-nearest-neighbor cells, supporting the scalability of

the symmetry-protected resonant shaking scheme for entanglement generation.

To realize a scalable cluster of bipartite entangled pairs in a superlattice with more unit cells, a prerequisite is the homogeneity of the lattice. In experiments, the overall harmonic confinement would lead to an inhomogeneous lattice and vary the resonant shaking frequency between unit cells. However, techniques to compensate for these confinement effects have been developed [40,41], which can be used to restore the homogeneity of the superlattice and ensure the scalability of the lattice shaking scheme.

B. Flexibility

The SPRSS also possesses the flexibility of generating an on-demand superposition of $|\pm\rangle$ by a combined shaking of V^+ and V^- . This on-demand generation resembles a rotation gate and has a potential use for $|\pm\rangle$ -based quantum computations. The generation of an on-demand superposition of $|\pm\rangle$ can be visualized by the appearance and rotation of a biwing structure in the profile of the two-body density. Figure 4 presents the two-body density profiles under the combined shaking $V^+ \pm 1.37V^-$ for two bosons in a double-well unit cell, where the factor 1.37 is due to the fact that under the same shaking amplitude $\langle +|V^+|G\rangle \approx 1.37\langle -|V^-|G\rangle$. The two-body density shown in Fig. 4(a) [Fig. 4(b)] indicates that the system resides in a state of $(|+\rangle \pm |-\rangle)/\sqrt{2} = |s, p\rangle$ ($|p, s\rangle$) by the corresponding combined shaking. These results exemplify the flexibility of the SPRSS, in terms of generating an on-demand superposition of $|\pm\rangle$.

C. Efficiency

Two main characteristics of the efficiency of the entanglement generation are the maximum fidelity of the targeted state and the preparation time to reach the maximum fidelity. We take the shaking V^- as an example and perform simulations on a single double-well unit cell to investigate the dependence of these two characteristics on the system parameters, among which we focus on the shaking amplitude, since the interaction strength mainly determines how well the whole system resides

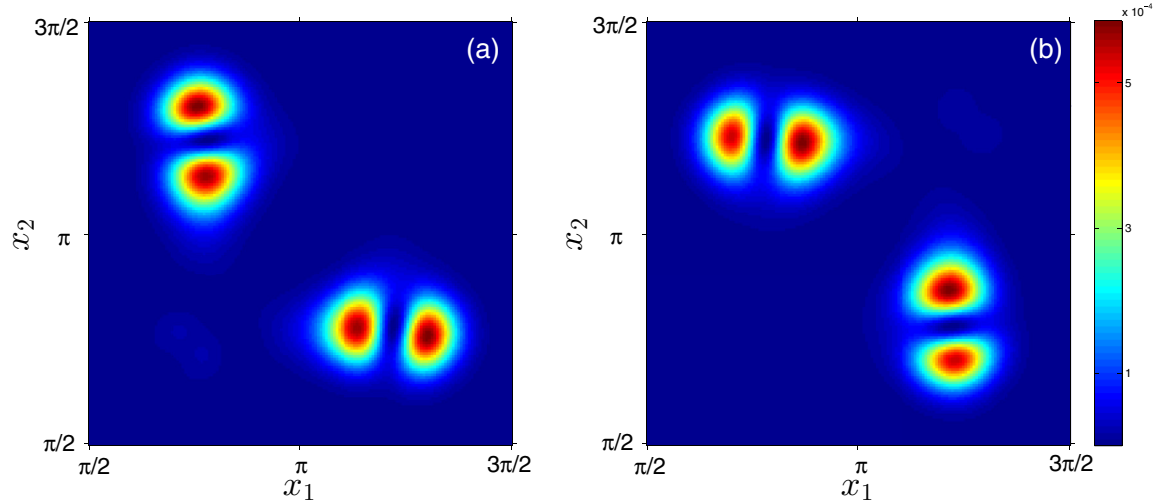


FIG. 4. Two-body density $\rho_2(x_1, x_2)$ under a combined shaking (a) $V^+ - 1.37V^-$ and (b) $V^+ + 1.37V^-$ at time $t = 294\hbar/E_R$, with the shaking amplitude $V_+ = V_- = 0.001$. The two figures share the same color bar.

in the Mott-like state $|G\rangle$. Figure 5(a) shows the maximum fidelity and the preparation time as a function of the shaking amplitude, where as the amplitude increases, the maximum

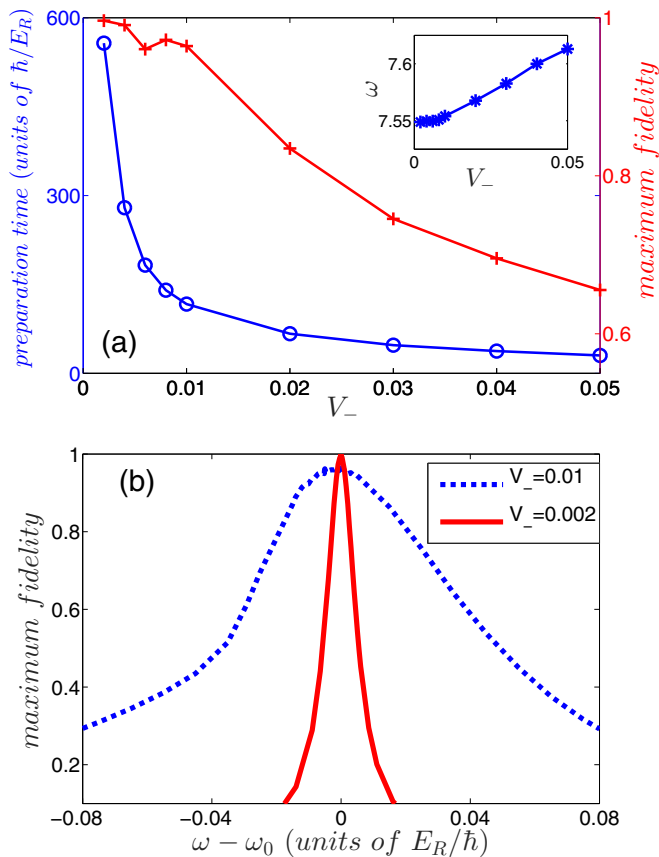


FIG. 5. (a) Maximum fidelity (right axis, line with pluses) and preparation time (left axis, line with circles) as a function of the shaking amplitude V_- . The inset shows the shaking frequency as a function of the shaking amplitude. (b) Maximum fidelity as a function of the frequency detuning for a shaking amplitude $V_- = 0.002$ (solid line) and $V_- = 0.01$ (dotted line).

fidelity and the preparation time both decrease. This can be understood since increasing the shaking amplitude, on the one hand, enhances the coupling between $|G\rangle$ and $|-\rangle$ and reduces the preparation time. On the other hand, a stronger shaking also activates eigenstates other than $|-\rangle$, which reduces the maximum fidelity. A further analysis shows that the shaking amplitude affects the preparation time more sensitively, as indicated in Fig. 5(a), i.e., when the shaking amplitude increases, for instance, from 0.001 to 0.005, the preparation time decreases almost by a factor of 5, from $550\hbar/E_R$ to $116\hbar/E_R$, and the maximum fidelity just decreases slightly from 99.6% to 96.4%. Figure 5(a) also reflects the robustness of the SPRSS.

The maximum fidelity as a function of the frequency detuning from the resonant frequency is also an important characteristic, due to the imperfect control of the shaking frequency in experiments. Figure 5(b) shows this dependence for different shaking amplitudes. For a stronger shaking amplitude, the maximum fidelity decreases more slowly with respect to the frequency detuning. Using the shaking scheme, it is therefore necessary to find a balance between the required maximum fidelity and preparation time, in order to optimize the shaking amplitude accordingly.

VI. CONCLUSION

We have developed and investigated a symmetry-protected resonant shaking scheme to generate scalable entangled states encoded within the orbital degrees of freedom of ultracold atoms in double-well superlattices. This scheme involves a first-order hopping process induced by a single operation of lattice shaking, which can significantly simplify the procedure of generating a cluster of bipartite entangled states. Moreover, the spatial symmetry of the orbital DOF endows this scheme with the capability of selective excitation of degenerate entangled states as well as the tunability to generate an on-demand superposition of them. The generated cluster of bipartite entangled states in the complete superlattice manifests as an alternative source for measurement-based quantum computations, for which various quantum gate operations

have been proposed [14,18–21]. Inspired by related works which focus on entangled states encoded in the spin DOF [16,42,43], the proposed entangled states can also be used for the investigations of dynamical transport of entanglement and the test of Bell inequalities. The lattice shaking scheme can be further optimized by engineering the temporal profile to increase the fidelity [44] and could also be applied to two-dimensional optical superlattices [45], where a true cluster state of maximum entanglement can be generated through resonant driving.

The orbital DOF also permits flexible manipulation and detection manners. For instance, direct lattice shaking can flip the orbitals, resembling the spin flipping through Raman pulses. Although a direct detection of the orbital state is difficult, the orbital state can be mapped to internal DOF or site occupations, for which well-developed techniques are ready for use. For instance, using spin-dependent superlattices can realize site- and orbital-resolved spin flipping [46] and map the orbital DOF to the internal DOF. Alternatively, one can map the s and p orbitals of one site to the d and f orbitals of the other site, and a subsequent band mapping [47–49] will count the particle numbers in different orbitals of the two sites. The rich manipulation and detection schemes strengthen the orbital DOF as a candidate in various applications.

ACKNOWLEDGMENTS

The authors acknowledge Jie Chen for his help in the numerical simulations. This work was supported by the National Natural Science Foundation of China (Grants No. 11625417 and No. 11604107). P.S. acknowledges financial support from the excellence cluster “The Hamburg Centre for Ultrafast Imaging—Structure, Dynamics, and Control of Matter at the Atomic Scale” of the Deutsche Forschungsgemeinschaft.

APPENDIX A: SELECTIVE EXCITATION THROUGH SYMMETRY-PROTECTED RESONANT SHAKINGS

The main goal of this work is to dynamically generate the targeted entangled states $|\pm\rangle$ from a given initial state $|G\rangle$, of which $|\pm\rangle$ and $|G\rangle$ are, to a good approximation, all eigenstates of the system. It is natural to think of using a resonant shaking potential to transport the system from the unentangled initial state to the desired entangled states, of which the shaking frequency matches the energy difference between the initial and the targeted states. This scheme, however, has the intrinsic difficulty that the targeted entangled states $|\pm\rangle$ are almost degenerate and an arbitrary shaking fulfilling the resonant condition cannot selectively excite one of the degenerate entangled states. It is even not guaranteed that such selective excitation through shaking is always possible. However, $|G\rangle$ and $|\pm\rangle$ possess a spatial two-body symmetry, which can be utilized to achieve the selective excitation. One can design particular shaking potentials which also possess this spatial symmetry and achieve a symmetry-protected selective excitation of the desired entangled states. In the following we will focus on two bosons confined in a double-well unit cell to demonstrate such two-body symmetry-protected selective excitation.

Let us first look at the wave functions of $|G\rangle$ and $|\pm\rangle$ to gain intuition of the spatial two-body symmetry. The wave functions of $|G\rangle$ and $|\pm\rangle$ for two bosons in a unit cell are denoted by $\psi_G(x_1, x_2)$ and $\psi_{\pm}(x_1, x_2)$, respectively, where x_1 and x_2 are the coordinates of the two bosons in the double-well unit cell. These functions $\psi_G(x_1, x_2)$ and $\psi_{\pm}(x_1, x_2)$ are shown in Fig. 6, in which the origin is set to the center of the unit cell. One obtains then $\psi_G(x_1, x_2) = \psi_G(-x_2, -x_1)$, $\psi_+(x_1, x_2) = -\psi_+(-x_2, -x_1)$, and $\psi_-(x_1, x_2) = \psi_-(-x_2, -x_1)$, which indicates that all wave functions possess a rotation symmetry along the line $x_1 + x_2 = 0$ in the configuration space spanned by x_1 and x_2 , i.e., a two-body exchange symmetry $x_1 \leftrightarrow -x_2$. Here $|G\rangle$ and $|-\rangle$ are of parity 1 with respect to this exchange symmetry, while $|+\rangle$ is of parity -1 . We define this two-body exchange as an operator $\hat{T} : x_i \leftrightarrow -x_{3-i}$ ($i = 1, 2$), with $\hat{T}|G\rangle = |G\rangle$, $\hat{T}|-\rangle = |-\rangle$, and $\hat{T}|+\rangle = -|+\rangle$. Then any shaking potential fulfilling the condition of $\hat{T}V\hat{T}^\dagger = +V$ ($-V$) will selectively couple $|G\rangle$ to $|-\rangle$ ($|+\rangle$). For instance, given a shaking potential with $\hat{T}V\hat{T}^\dagger = V$, we have

$$\langle +|V|G\rangle = -\langle +|\hat{T}^\dagger(\hat{T}V\hat{T}^\dagger)(\hat{T}|G\rangle) = -\langle +|V|G\rangle = 0 \quad (\text{A1})$$

and this shaking potential can only couple $|G\rangle$ to $|-\rangle$ and realize a selective excitation of $|-\rangle$. Similarly, we can prove that a shaking potential with $\hat{T}V\hat{T}^\dagger = -V$ can only couple $|G\rangle$ to $|+\rangle$ and realize the selective excitation of $|+\rangle$. It can be verified that the shaking potentials V^+ and V^- fulfill the conditions $\hat{T}V^+\hat{T}^\dagger = -V^+$ and $\hat{T}V^-\hat{T}^\dagger = V^-$, which enables for V^+ and V^- the selective excitation of $|+\rangle$ and $|-\rangle$, respectively.

Above we have provided an intuitive approach to the two-body exchange symmetry for $|G\rangle$ and $|\pm\rangle$. This can be done more rigorously by analyzing the analytical form of the wave functions. Approximating each well as a harmonic trap, we can write the wave functions as

$$\begin{aligned} \psi_G(x_1, x_2) &= \frac{\alpha}{\pi^{1/2}} e^{-\alpha^2[(x_1-x_L)^2+(x_2-x_R)^2]/2} + (x_1 \leftrightarrow x_2), \\ \psi_+(x_1, x_2) &= \frac{\sqrt{2}\alpha}{\pi^{1/2}} (x_1 + x_2) e^{-\alpha^2[(x_1-x_L)^2+(x_2-x_R)^2]/2} \\ &\quad + (x_1 \leftrightarrow x_2), \\ \psi_-(x_1, x_2) &= \frac{\sqrt{2}\alpha}{\pi^{1/2}} (x_1 - x_2) e^{-\alpha^2[(x_1-x_L)^2+(x_2-x_R)^2]/2} \\ &\quad + (x_1 \leftrightarrow x_2). \end{aligned} \quad (\text{A2})$$

In Eqs. (A2), x_L and x_R refer to the local minimum in the left and right wells, respectively, and $x_L = -x_R$. In addition, $\alpha \equiv \sqrt{\omega_0/\hbar}$ is the normalization factor, with ω_0 being the effective confining frequency of the left and right well. Further, $(x_1 \leftrightarrow x_2)$ denotes the permutation of x_1 and x_2 in the related wave function. The wave functions in Eqs. (A2) directly give $\hat{T}|G\rangle = |G\rangle$ and $\hat{T}|\pm\rangle = \mp|\pm\rangle$ in deep lattices.

APPENDIX B: ANSATZ AND ANALYSIS OF THE ML-MCTDHX

To demonstrate the validity of the resonant shaking scheme, we perform *ab initio* numerical simulations of the dynamical process of shaking. The method applied here is the

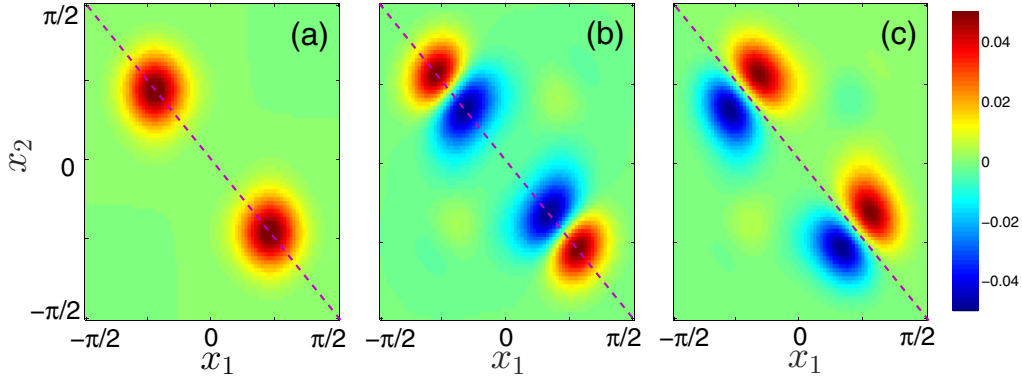


FIG. 6. Wave function of two bosons in a double-well unit cell, in the eigenstates (a) $|G\rangle$, (b) $|-\rangle$, and (c) $|+\rangle$. The origin is chosen to be the center of the unit cell. The dotted lines in the figures indicate the rotation axis of \hat{T} .

ML-MCTDHX. The ML-MCTDHX accounts for all correlations among the bosons and can intrinsically take into account the exact geometry of the 1D superlattice and the parity of the shaking potentials, which turns out to be essential for the generation scheme in this work. The atoms in the superlattice are taken as a closed system and effects due to finite but sufficiently low temperature and/or spontaneous emission are ignored, which, however, we believe will not affect the main results of this work.

In simulating the shaking dynamics in this work, the first step of the method is to construct a set of single-particle basis functions of the discrete-variable representation (DVR) type. In our simulations, we adopted the exponential DVR [32], which corresponds to discretizing the continuous interval $[x_i, x_f]$ into a set of grid points $\{x_i + (n-1)\delta x\}_{n=1}^G$, with $\delta x = (x_f - x_i)/(G-1)$. Each grid point, e.g., x , is associated with a DVR basis function $\phi(x)$, which approximates a δ function located at the grid point x . The corresponding annihilation (creation) operator $\hat{\phi}(x)$ [$\hat{\phi}^\dagger(x)$] then denotes annihilating (creating) a boson at the corresponding grid point. When the set of grid points is sufficient dense, it can well approximate the continuous space.

In the next step, we assign to the identical bosons a set of time-dependent single-particle functions (SPFs) $\{|\psi_i(x, t)\rangle\}_{i=1}^m$ and each SPF is associated with an annihilation (creation) operator $\{\hat{a}_i\}$ ($\{\hat{a}_i^\dagger\}$) as

$$\begin{aligned}\hat{a}_i &= \sum_{x \in [x_i, x_f]} \psi_i(x, t) \phi(x), \\ \hat{a}_i^\dagger &= \sum_{x \in [x_i, x_f]} \psi_i(x, t) \phi^\dagger(x).\end{aligned}\quad (\text{B1})$$

The SPFs span a set of Fock states for the $2N$ bosons confined in a superlattice with N unit cells $\{|\vec{n}\rangle = |(n_1, n_2, \dots, n_m)\rangle\}$, with n_i denoting the occupation of the i th SPF and $n_1 + n_2 + \dots + n_m = 2N$. The Fock state $|\vec{n}\rangle$ is defined in the standard second-quantization manner

$$|\vec{n}\rangle = \sqrt{\frac{1}{n_1! n_2! \dots n_m!}} \prod_{i \in [1, m]} (\hat{a}_i^\dagger)^{n_i} |\text{vac}\rangle, \quad (\text{B2})$$

where $|\text{vac}\rangle$ denotes the vacuum state.

Then the total wave function of the system becomes

$$|\Psi(t)\rangle = \sum_{\vec{n}} C_{\vec{n}}(t) |\vec{n}\rangle. \quad (\text{B3})$$

Equations (3)–(5) constitute the complete wave-function ansatz of the ML-MCTDHX. Substituting the ansatz into the Dirac-Frenkel variational principle, we can obtain the equations of motion for the total wave function and resultingly the time evolution of the system.

In our analysis, besides the $g^{(2)}$ function, we mainly rely on the projection of the total wave function $|\Psi(t)\rangle$ to different eigenstates $|\alpha\rangle$, where $|\alpha\rangle$ denotes the eigenstates of our interest, e.g., $|G\rangle$ and $|\pm\rangle$. The projection is calculated with the following procedure. First we define a set of time-independent single-particle functions, which are normalized and orthogonal to each other. This set of single-particle functions spans a set of time-independent Fock states $|\vec{n}\rangle_s$. We can then project the total wave function $|\Psi(t)\rangle$ and $|\alpha\rangle$ to the time-independent Fock basis and further obtain the projection of $|\Psi(t)\rangle$ to $|\alpha\rangle$ as

$$\langle \alpha | \Psi(t) \rangle = \sum_{\vec{n}} \langle \alpha | \vec{n} \rangle_s \langle \vec{n} | \Psi(t) \rangle. \quad (\text{B4})$$

A sufficient condition for the validity of Eq. (B4) is that $|\Psi(t)\rangle$ and $|\alpha\rangle$ lie within the Fock basis spanned by the time-independent single-particle functions, i.e., $\sum_{\vec{m}} |s\rangle \langle \vec{m} | \Psi \rangle|^2 \approx 1$ and $\sum_{\vec{m}} |s\rangle \langle \vec{m} | \alpha \rangle|^2 \approx 1$. This sufficient condition is well checked and fulfilled in our analysis. A further comment on the choice of the time-independent single-particle functions is that these functions can be chosen as the Wannier states or the eigenstates of a single particle in the superlattice and our experience shows that the latter provides a better performance. This is due to the fact that the practical definition of Wannier functions suffers intrinsic uncertainties, which could lead to false fluctuations in the projection analysis, while the eigenstates of single particles are obtained by direct diagonalization and are more robust.

APPENDIX C: CONVERGENCE

The ML-MCTDHX manifests itself as an *ab initio* numerical method for many-body quantum systems and it takes into account all quantum correlations within the system. Assuming

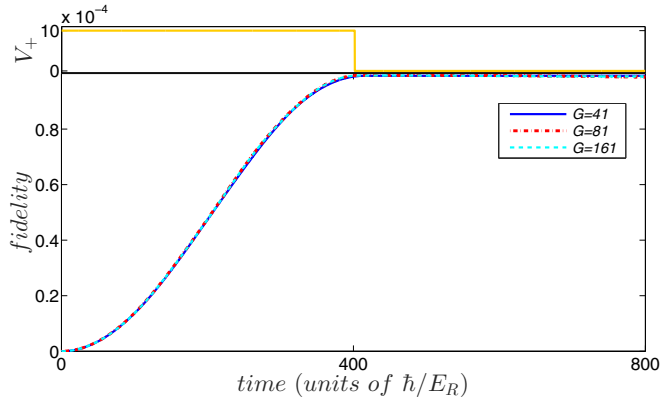


FIG. 7. Fidelity of $|\langle +|\Psi(t)\rangle|^2$ under shaking V^+ for two bosons in a double-well unit cell, with $G = 41$ (blue solid line), $G = 81$ (red dot-dashed line), and $G = 161$ (cyan dashed line). The upper panel shows the temporal profile of the shaking amplitude.

convergence, the ML-MCTDHX provides the numerically exact dynamical process of the system in consideration. The convergence of the simulation is mainly determined by the two control parameter in the wave-function ansatz, namely, the number of grid points G and the number of SPFs m . In the setup, G should be large enough for the discrete grid points to well approximate the continuous space. The size of SPFs m must be sufficiently large to well characterize the quantum correlations of the system.

To determine the convergence in terms of G , we can directly compare the numerical results for different G . Convergence is reached if the results remain, to some desired precision, the same as G increases. Figure 7 compares the temporal evolution of the fidelity of $|\langle +|\Psi(t)\rangle|^2$ under the shaking V^+ in a single double-well unit cell with $G = 41$, 81, and 161. It can be seen that the curves for different G almost lie on top of each other, which indicates a good convergence for using 41 grid points per unit cell, which is what we apply in our simulations.

It is also important to verify the convergence in terms of the number of SPFs, which demonstrates how accurately quantum correlations are taken into account. A well-accepted strategy to verify the convergence with respect to m is through the natural population of the system. More specifically, the one-body density matrix is calculated during the dynamics and is diagonalized to obtain the so-called natural orbitals and natural populations, which are the eigenstates and corresponding eigenvalues of the one-body density matrix, respectively. A signature of convergence with respect to m is that the lowest natural populations in the dynamical process are close to zero, which indicates that abundant SPFs have been supplied for the calculation and quantum correlations are adequately taken into account. For this purpose, we calculate the natural populations during the shaking dynamics of two bosons in a single unit cell [Fig. 8(a)] with $m = 4$ and 6, as well as those of four bosons in two cells with $m = 8$ and 12 [Fig. 8(b)]. Comparing the natural populations for $m = 4$ and 6 in Fig. 8(a), one can see

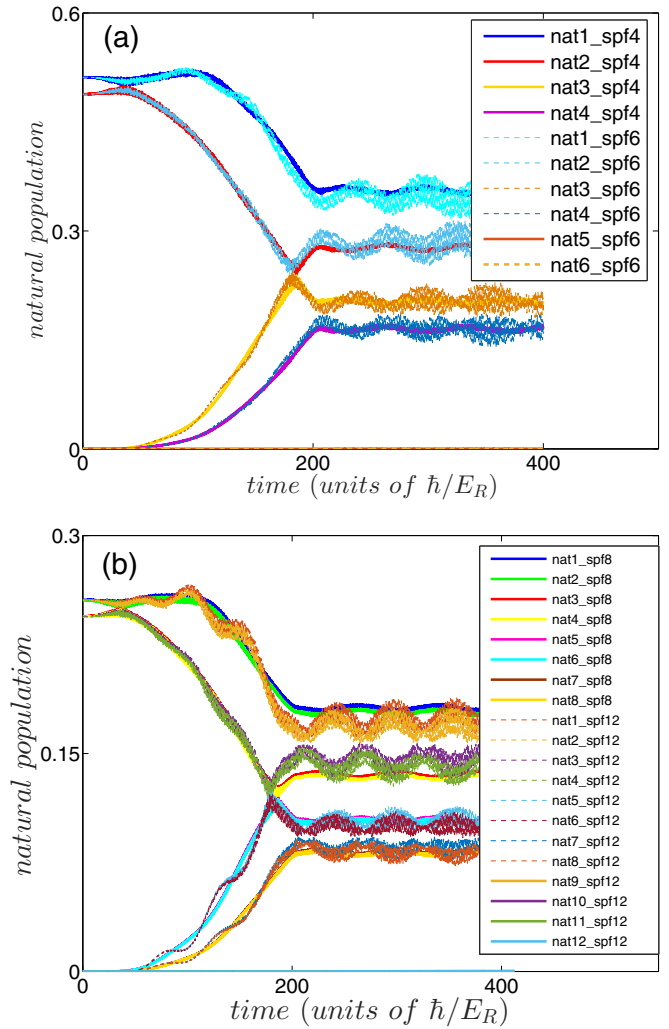


FIG. 8. Temporal evolution of the natural populations in (a) the single-cell and (b) the double-cell setup. In the single-cell case, $m = 4$ and $m = 6$, and in the double-cell case, $m = 8$ and $m = 12$ are used for comparison.

that only four natural orbitals are significantly occupied and the natural populations of the remaining two natural orbitals are very small. The natural-population profiles of the occupied natural orbitals in the setup of $m = 6$ lie on top of the profiles of the corresponding natural populations of the setup for $m = 4$, despite numerical fluctuations. Both indicate that it is sufficient to supply four SPFs for a single-cell simulation. In Fig. 8(b) we observe a similar temporal behavior of the natural populations, which indicates that eight SPFs are sufficient for four bosons in two double-well unit cells. The convergence diagnosis in both the single and the double unit-cell setups indicates that four SPFs per unit cell can give very-well-converged results for the dynamics. Nevertheless, in the simulations shown in the main text for setups of single and double unit cells, we employ six SPFs per unit cell to obtain a higher precision. Only in the simulation with three unit cells, we employ four SPFs per unit cell.

- [1] I. Bloch, *Nat. Phys.* **1**, 23 (2005).
- [2] I. Bloch, J. Dalibard, and W. Zwerger, *Rev. Mod. Phys.* **80**, 885 (2008).
- [3] X.-Y. Luo, Y.-Q. Zou, L.-N. Wu, Q. Liu, M.-F. Han, M. K. Tey, and L. You, *Science* **355**, 620 (2017).
- [4] D. Jaksch, H.-J. Briegel, J. I. Cirac, C. W. Gardiner, and P. Zoller, *Phys. Rev. Lett.* **82**, 1975 (1999).
- [5] G. K. Brennen, C. M. Caves, P. S. Jessen, and I. H. Deutsch, *Phys. Rev. Lett.* **82**, 1060 (1999).
- [6] H. J. Briegel, D. E. Browne, W. Dur, R. Raussendorf, and M. Van den Nest, *Nat. Phys.* **5**, 19 (2009).
- [7] H. J. Briegel and R. Raussendorf, *Phys. Rev. Lett.* **86**, 910 (2001).
- [8] L. Jiang, A. M. Rey, O. Romero-Isart, J. J. García-Ripoll, A. Sanpera, and M. D. Lukin, *Phys. Rev. A* **79**, 022309 (2009).
- [9] T. Calarco, E. A. Hinds, D. Jaksch, J. Schmiedmayer, J. I. Cirac, and P. Zoller, *Phys. Rev. A* **61**, 022304 (2000).
- [10] O. Mandel, M. Greiner, A. Widera, T. Rom, T. W. Hänsch, and I. Bloch, *Nature (London)* **425**, 937 (2003).
- [11] L.-M. Duan, E. Demler, and M. D. Lukin, *Phys. Rev. Lett.* **91**, 090402 (2003).
- [12] M. Anderlini, P. J. Lee, B. L. Brown, J. Sebby-Strabley, W. D. Phillips, and J. V. Porto, *Nature (London)* **448**, 452 (2007).
- [13] S. Trotzky, P. Cheinet, S. Fölling, M. Feld, U. Schnorrberger, A. M. Rey, A. Polkovnikov, E. A. Demler, M. D. Lukin, and I. Bloch, *Science* **319**, 295 (2008).
- [14] B. Vaucher, A. Nunnenkamp, and D. Jaksch, *New J. Phys.* **10**, 023005 (2008).
- [15] A. M. Kaufman, B. J. Lester, M. Foss-Feig, M. L. Wall, A. M. Rey, and C. A. Regal, *Nature (London)* **527**, 208 (2015).
- [16] H.-N. Dai, B. Yang, A. Reingruber, X.-F. Xu, X. Jiang, Y.-A. Chen, Z.-S. Yuan, and J.-W. Pan, *Nat. Phys.* **12**, 783 (2016).
- [17] X. Li and W. V. Liu, *Rep. Prog. Phys.* **79**, 116401 (2016).
- [18] E. Charron, E. Tiesinga, F. Mies, and C. Williams, *Phys. Rev. Lett.* **88**, 077901 (2002).
- [19] K. Eckert, J. Mompert, X. X. Yi, J. Schliemann, D. Bruß, G. Birkel, and M. Lewenstein, *Phys. Rev. A* **66**, 042317 (2002).
- [20] F. W. Strauch, M. Edwards, E. Tiesinga, C. Williams, and C. W. Clark, *Phys. Rev. A* **77**, 050304 (2008).
- [21] P.-I. Schneider and A. Saenz, *Phys. Rev. A* **85**, 050304 (2012).
- [22] K. Inaba, Y. Tokunaga, K. Tamaki, K. Igeta, and M. Yamashita, *Phys. Rev. Lett.* **112**, 110501 (2014).
- [23] J. Struck, C. Ölschläger, M. Weinberg, P. Hauke, J. Simonet, A. Eckardt, M. Lewenstein, K. Sengstock, and P. Windpassinger, *Phys. Rev. Lett.* **108**, 225304 (2012).
- [24] N. Fläschner, B. S. Rem, M. Tarnowski, D. Vogel, D.-S. Lühmann, K. Sengstock, and C. Weitenberg, *Science* **352**, 1091 (2016).
- [25] N. Goldman and J. Dalibard, *Phys. Rev. X* **4**, 031027 (2014).
- [26] S. Trotzky, Y.-A. Chen, U. Schnorrberger, P. Cheinet, and I. Bloch, *Phys. Rev. Lett.* **105**, 265303 (2010).
- [27] Y.-A. Chen, S. Nascimbène, M. Aidelsburger, M. Atala, S. Trotzky, and I. Bloch, *Phys. Rev. Lett.* **107**, 210405 (2011).
- [28] A. Eckardt, *Rev. Mod. Phys.* **89**, 011004 (2017).
- [29] S. Krönke, L. Cao, O. Vendrell, and P. Schmelcher, *New J. Phys.* **15**, 063018 (2013).
- [30] L. Cao, S. Krönke, O. Vendrell, and P. Schmelcher, *J. Chem. Phys.* **139**, 134103 (2013).
- [31] L. Cao, V. Bolsinger, S. I. Mistakidis, G. M. Koutentakis, S. Krönke, J. M. Schurer, and P. Schmelcher, *J. Chem. Phys.* **147**, 044106 (2017).
- [32] H.-D. Meyer, U. Manthe, and L. Cederbaum, *Chem. Phys. Lett.* **165**, 73 (1990).
- [33] M. H. Beck, A. Jäckle, G. A. Worth, and H. D. Meyer, *Phys. Rep.* **324**, 1 (2000).
- [34] U. Manthe, *J. Chem. Phys.* **128**, 164116 (2008).
- [35] O. Vendrell and H.-D. Meyer, *J. Chem. Phys.* **134**, 044135 (2011).
- [36] O. E. Alon, A. I. Streltsov, and L. S. Cederbaum, *Phys. Rev. A* **77**, 033613 (2008).
- [37] O. E. Alon, A. I. Streltsov, and L. S. Cederbaum, *J. Chem. Phys.* **140**, 034108 (2014).
- [38] O. E. Alon, A. I. Streltsov, K. Sakmann, A. U. Lode, J. Grond, and L. S. Cederbaum, *Chem. Phys.* **401**, 2 (2012).
- [39] R. Jozsa, *J. Mod. Opt.* **41**, 2315 (1994).
- [40] S. Will, T. Best, U. Schneider, L. Hackermüller, D.-S. Lühmann, and I. Bloch, *Nature (London)* **465**, 197 (2010).
- [41] A. Mazurenko, C. S. Chiu, G. Ji, M. F. Parsons, M. Kanász-Nagy, R. Schmidt, F. Grusdt, E. Demler, D. Greif, and M. Greiner, *Nature (London)* **545**, 462 (2017).
- [42] T. Keilmann and J. J. García-Ripoll, *Phys. Rev. Lett.* **100**, 110406 (2008).
- [43] P. Barmettler, A. M. Rey, E. Demler, M. D. Lukin, I. Bloch, and V. Gritsev, *Phys. Rev. A* **78**, 012330 (2008).
- [44] D. Gagnon, F. Fillion-Gourdeau, J. Dumont, C. Lefebvre, and S. MacLean, *Phys. Rev. Lett.* **119**, 053203 (2017).
- [45] A. Kiely, A. Benseny, T. Busch, and A. Ruschhaupt, *J. Phys. B* **49**, 215003 (2016).
- [46] B. Yang, H.-N. Dai, H. Sun, A. Reingruber, Z.-S. Yuan, and J.-W. Pan, *Phys. Rev. A* **96**, 011602 (2017).
- [47] A. Kastberg, W. D. Phillips, S. L. Rolston, R. J. C. Spreeuw, and P. S. Jessen, *Phys. Rev. Lett.* **74**, 1542 (1995).
- [48] S. Fölling, S. Trotzky, P. Cheinet, M. Feld, R. Saers, A. Widera, T. Müller, and I. Bloch, *Nature (London)* **448**, 1029 (2007).
- [49] P. Cheinet, S. Trotzky, M. Feld, U. Schnorrberger, M. Moreno-Cardoner, S. Fölling, and I. Bloch, *Phys. Rev. Lett.* **101**, 090404 (2008).